Supplementary information

Investigating the asymmetric electrochemical, structural and electronic properties of Mn-rich Li(Mn,Fe)PO_4 electrode materials

Beatrice Ricci[a,b,c]*, Felix-Cosmin Mocanu[a], Dimitrios Chatzogiannakis[b,d], Victor Fuentes[b,d], Ashley P. Black[b,d], Benoît Cluzeau[e], Cécile Tessier[e], Patrick Bernard[e], M. Saiful Islam[a,c]*, M. Rosa Palacín[b,c]*

Electrochemical performance

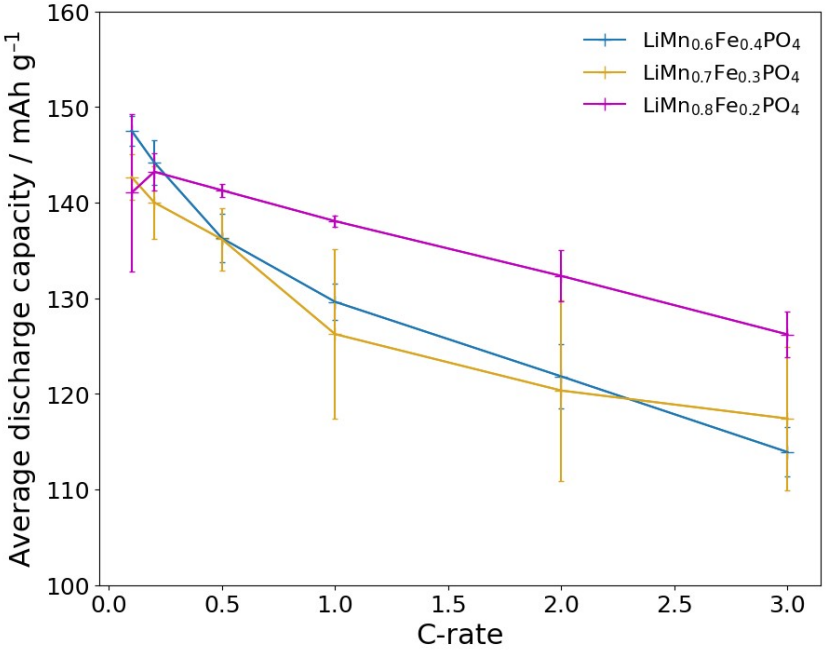

Figure S1: *Average discharge capacities obtained over 4 trials at different rates in coin cells against Li metal with 1M $LiPF_6$ in 1:1 EC/DMC electrolyte cycled between 2.5 and 4.3 V vs Li^+/Li prior to the half hour hold at the voltage cutoff. Rate of 1C is equivalent to full (de)lithiation in 1 hour (~3 mA current), calculated based off a theoretical capacity of 170 mAh g^{-1}.*

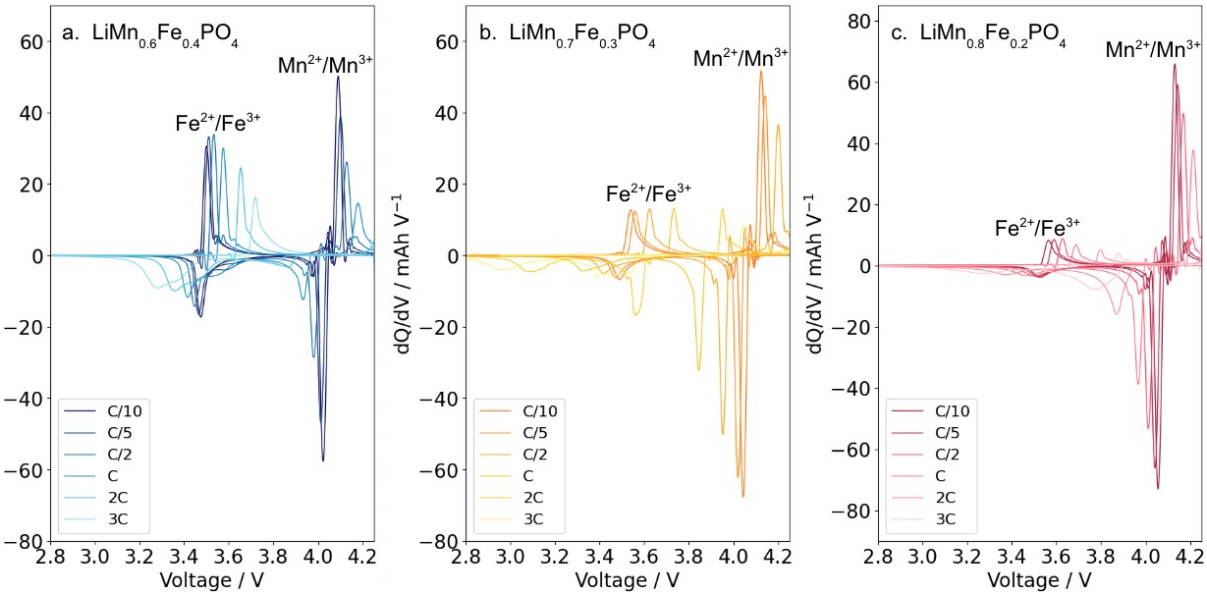

Figure S2: *dQ/dV calculated from constant-current galvanostatic cycling capacity and voltage data at different rates in coin cells against Li metal with 1M LiPF6 in 1:1 EC/DMC electrolyte cycled between 2.5 and 4.3 V vs Li^+/Li. Rate of 1C is equivalent to full charge in 1 hour (~3 mA current).*

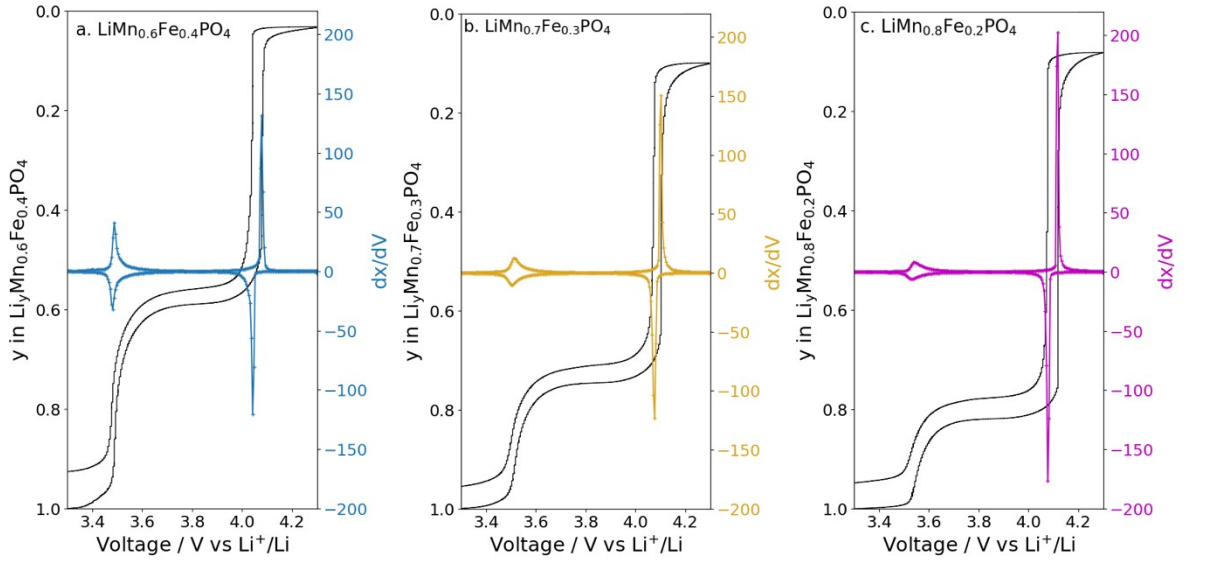

Figure S3: *Incremencal capacity voltammograms (blue) and charge-discharge profiles (black) for a. $LiMn_{0.6}Fe_{0.4}PO_4$, b. $LiMn_{0.7}Fe_{0.3}PO_4$, and c. $LiMn_{0.8}Fe_{0.2}PO_4$ measured in 2032-type coin cells vs. lithium using PITT.*

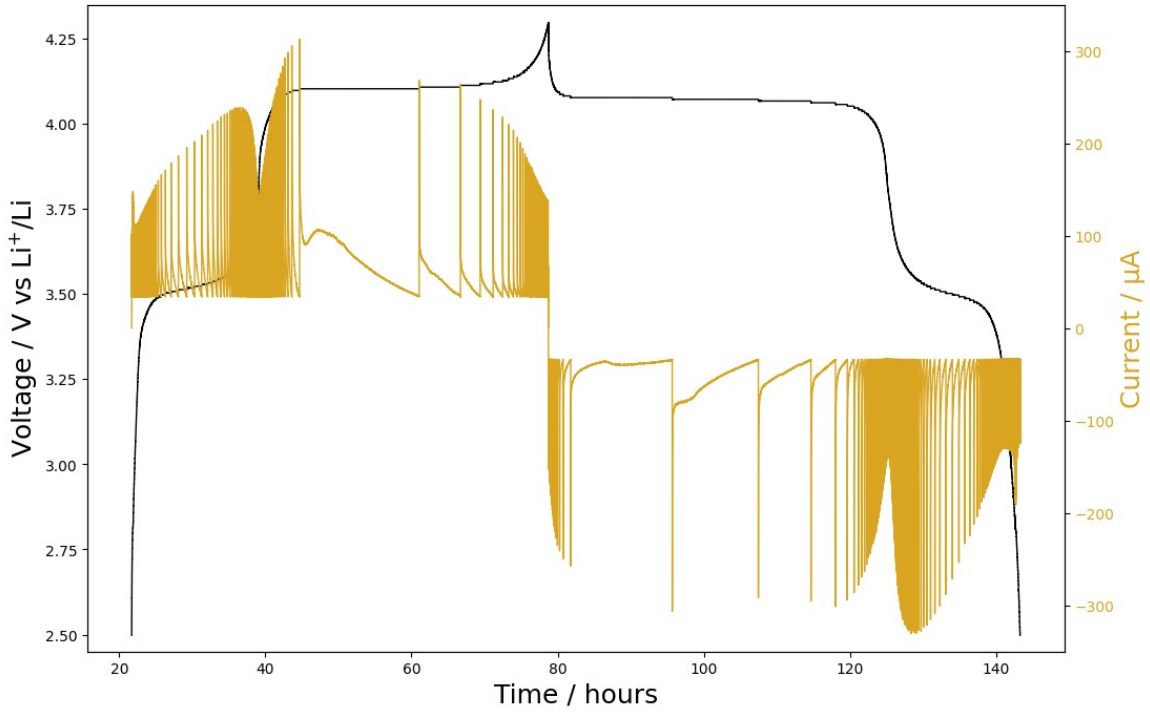

Figure S4: *Stepped PITT voltage profile and current response for $LiMn_{0.7}Fe_{0.3}PO_4$ measured in 2032-type coin cells vs. lithium.*

Operando X-ray diffraction and absorption near edge spectra

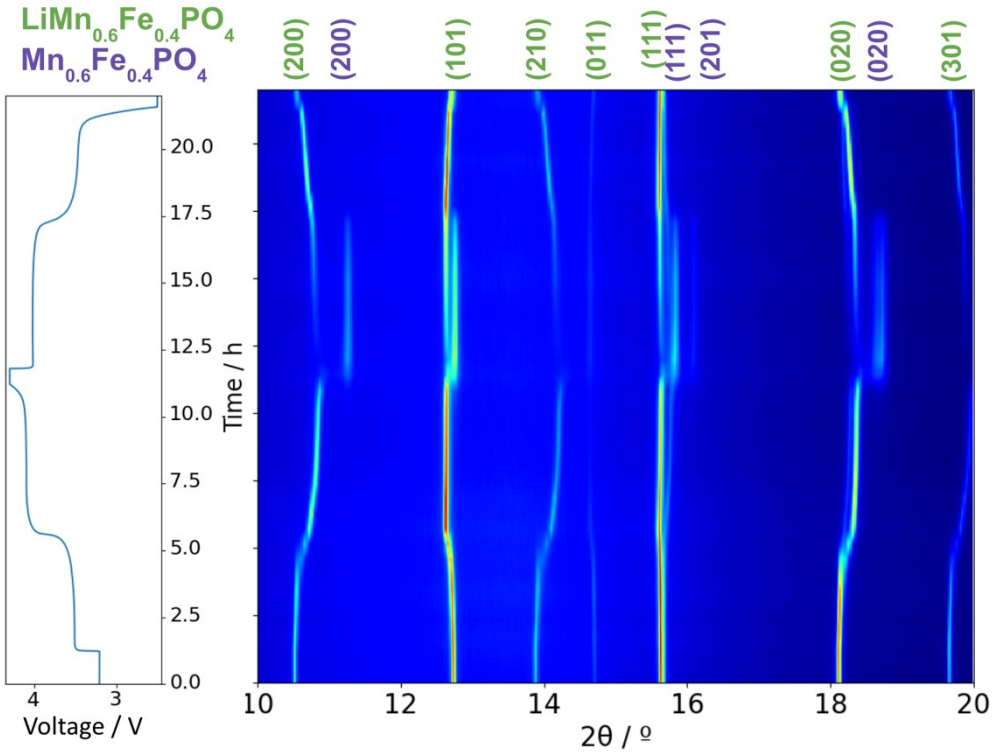

Figure S5: a. *Synchrotron* operando *X-ray diffraction patterns in the 2ϑ = 10 – 20 º region for one full cycle at C/10 of the LMFP64 cell recorded at 13 keV (λ = 0.952729 Å) with the respective voltage profile. The reflections corresponding to both the lithiated and delithiated phases are depicted.*

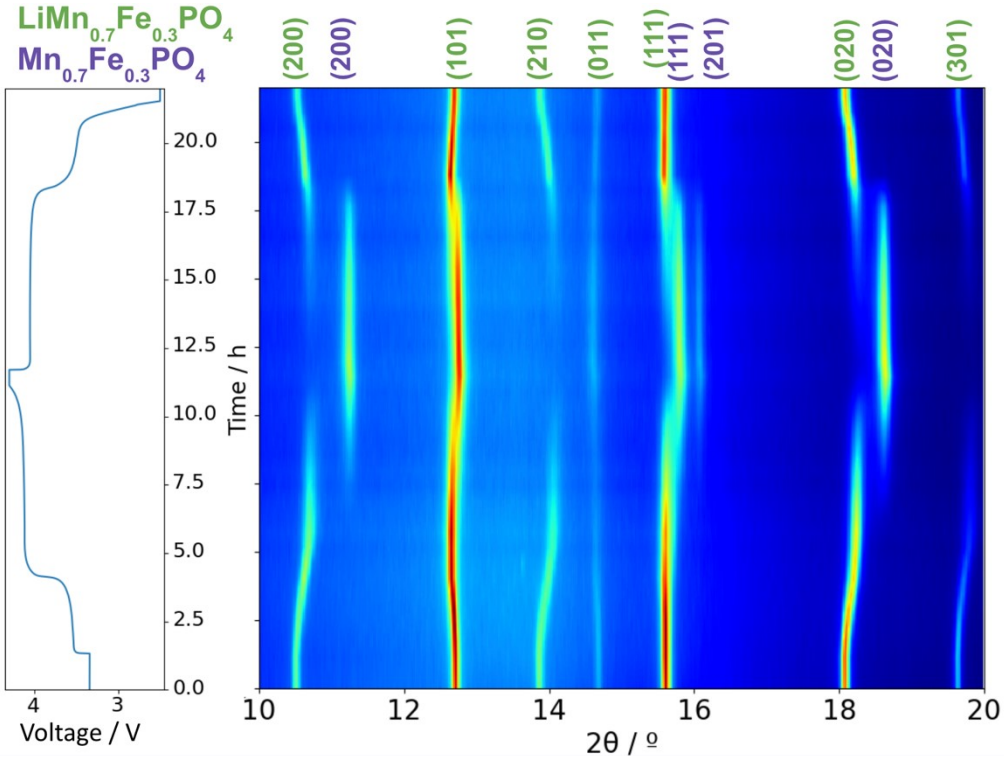

Figure S5: b. *Synchrotron* operando *X-ray diffraction patterns in the 2ϑ = 10 – 20 º region for one full cycle at C/10 of the LMFP73 cell recorded at 13 keV (λ = 0.952729 Å) with the respective voltage profile. The reflections corresponding to both the lithiated and delithiated phases are depicted.*

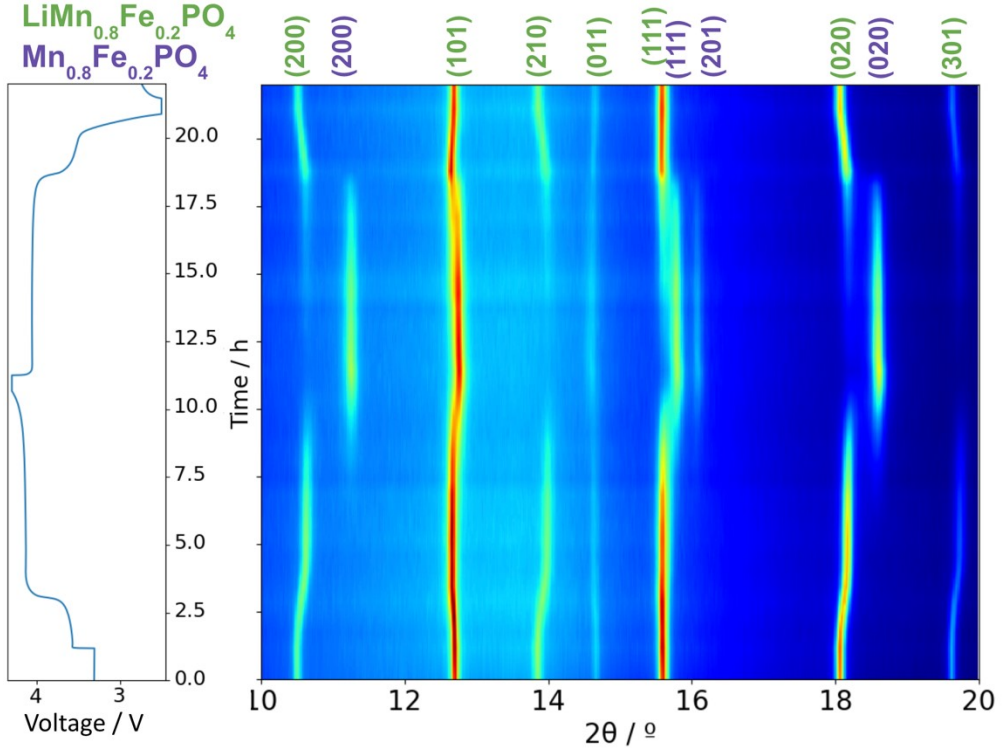

Figure S5: c. *Synchrotron* operando *X-ray diffraction patterns in the 2ϑ = 10 – 20 º region for one full cycle at C/10 of the LMFP82 cell recorded at 13 keV (λ = 0.952729 Å) with the respective voltage profile. The reflections corresponding to both the lithiated and delithiated phases are depicted.*

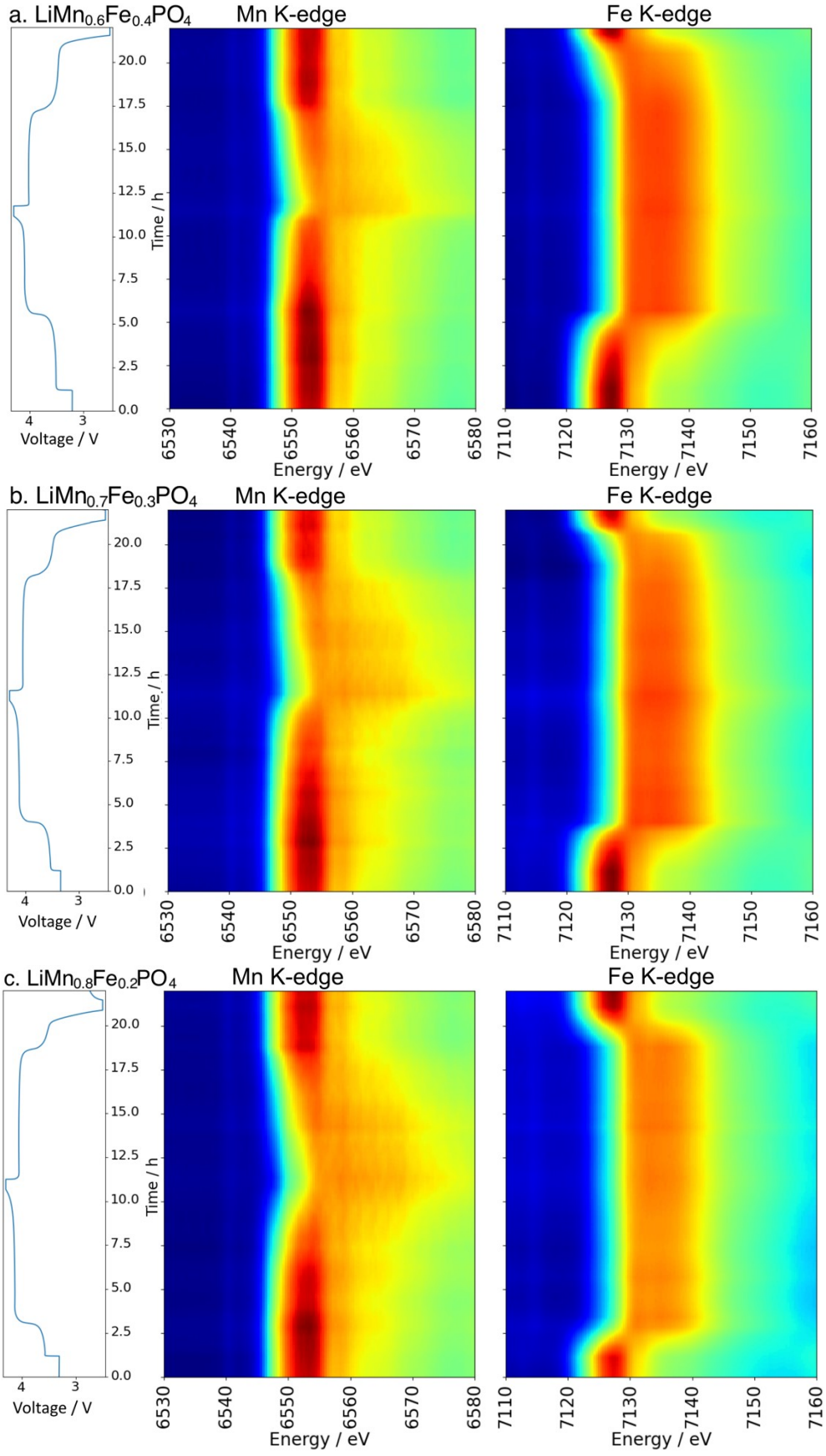

Figure S6: operando *XAS absorption spectra at the Mn and Fe K-edges for a. x = 0.6, b. x = 0.7, c. x = 0.8 during cycling at C/10.*

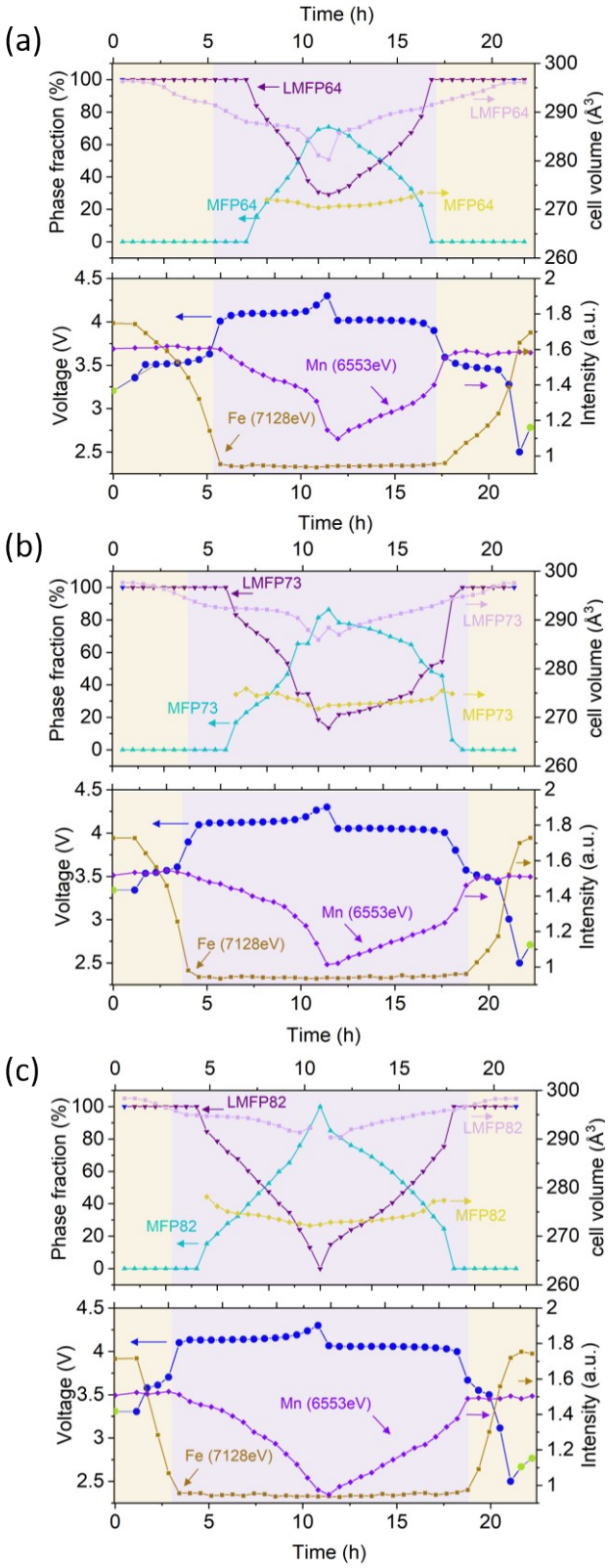

***Figure S7**: Phase fractions and cell volumes obtained from sequential Rietveld refinements of operando X-ray diffraction patterns, together with X-ray absorption intensities at selected energies near the Mn and Fe K-edges. All data are correlated with the corresponding cell voltage recorded during data acquisition for $LiMn_xFe_{1-x}PO_4$ with: (a) x = 0.6, (b) x = 0.7, and (c) x = 0.8. Phase fraction information from Rietveld refinement was used to identify the lithiation ranges across which solid-solution and two-phase behaviour take place, as depicted in Figure 5.*

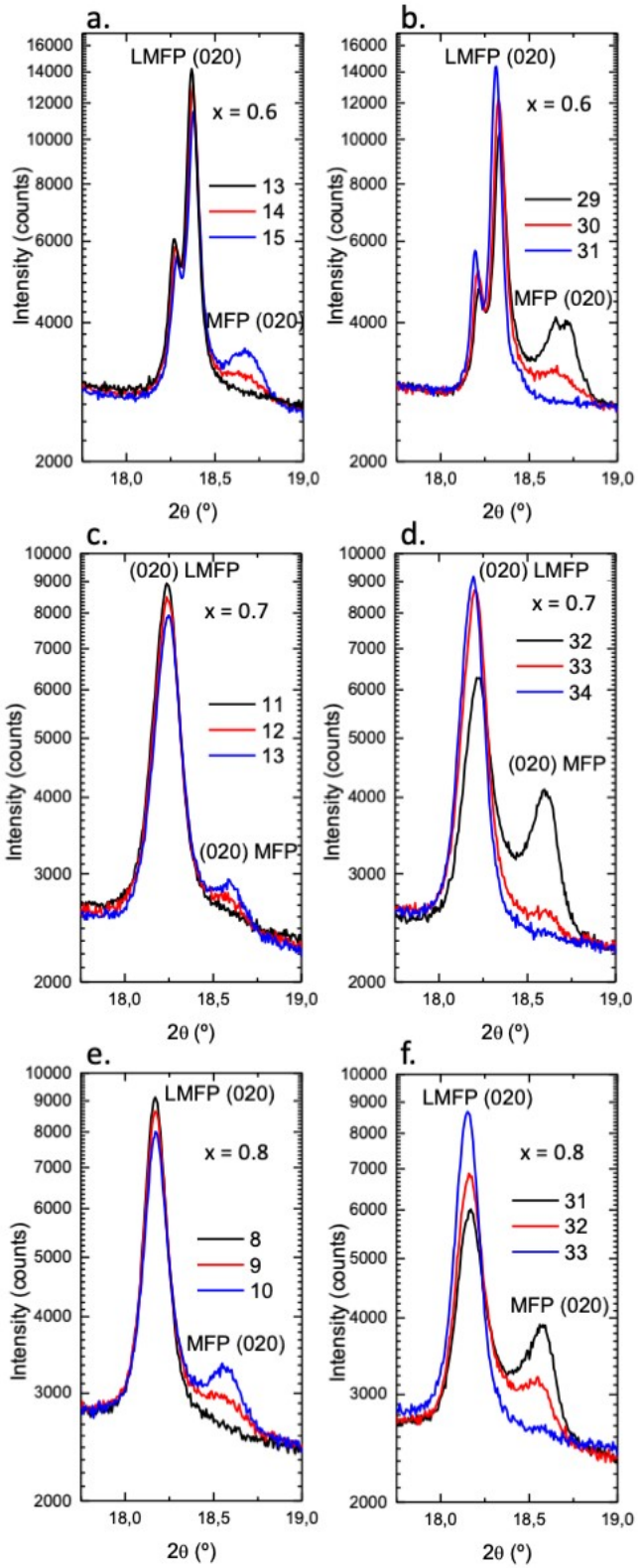

***Figure S8**: Diffraction patterns corresponding to the transitions between solid-solution and two-phase regimes for $LiMn_xFe_{1-x}PO_4$ for a. x = 0.6, charge; b. x = 0.6, discharge; c. x = 0.7, charge; d. x = 0.7, discharge; e. x = 0.8, charge; f. x = 0.8, discharge.*

Atomistic insights into defects and ion migration

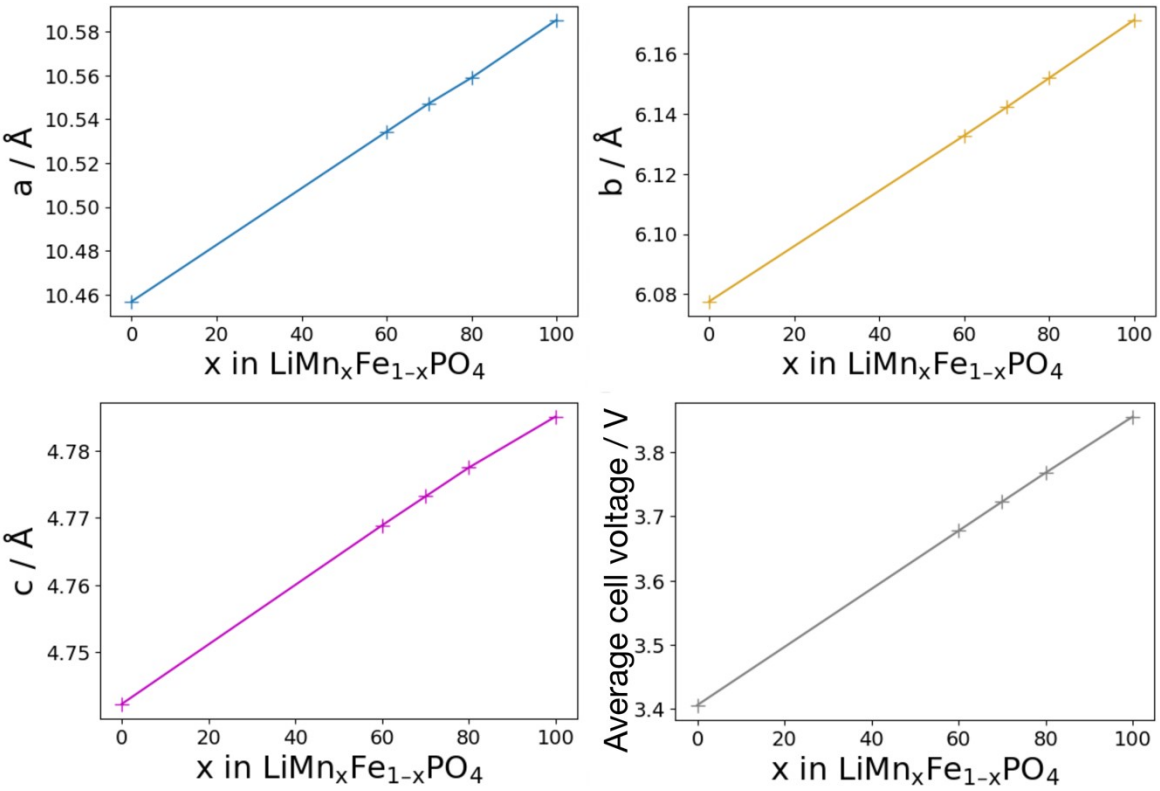

***Figure S9**: Calculated crystallographic a.* a *lattice parameter, b.* b *lattice parameter, c.* c *lattice parameter, and d. average cell voltage versus lithium with increasing x in* $LiMn_xFe_{1-x}PO_4$

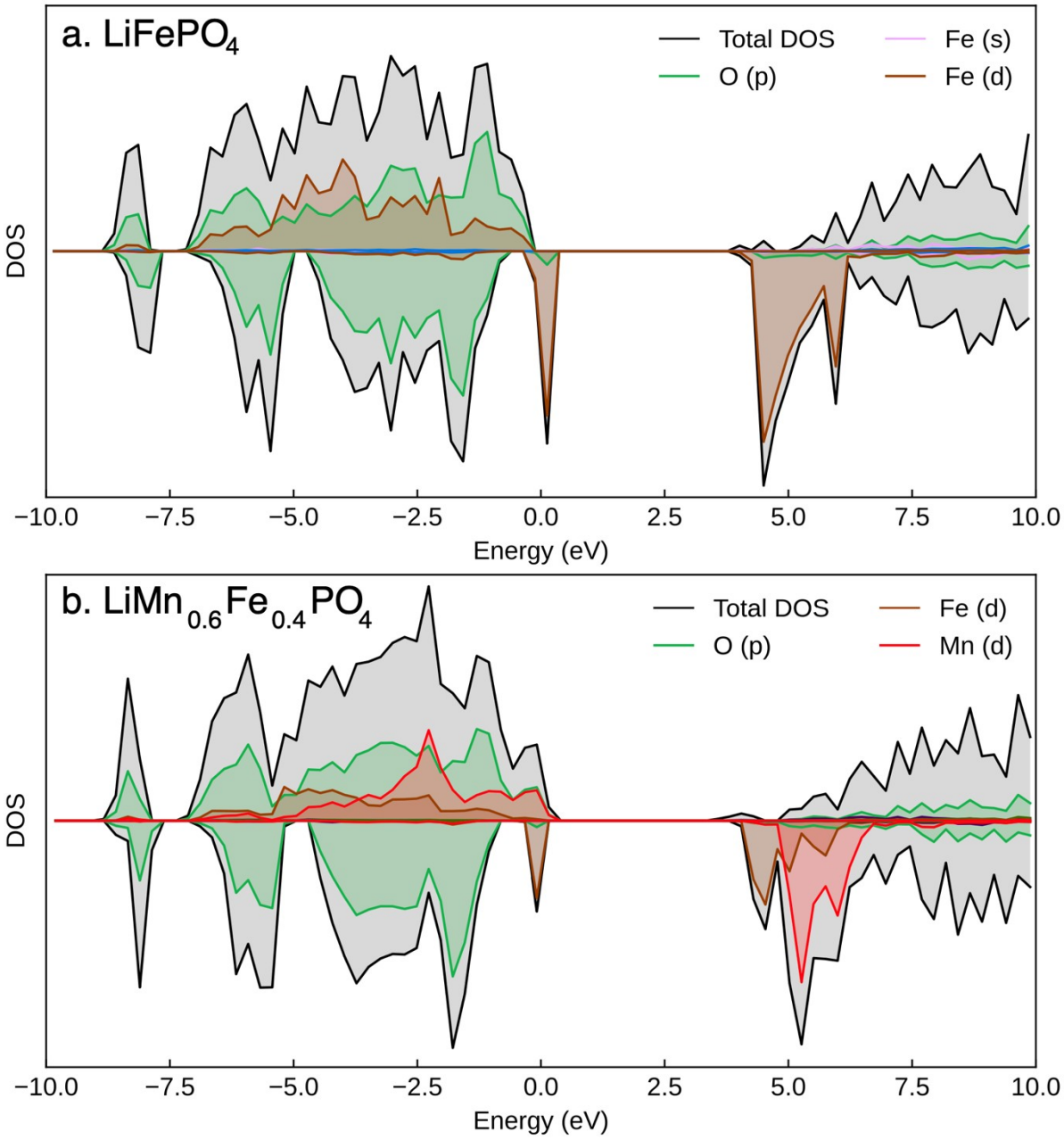
a. LiFePO4
Total DOS
Fe (s)
O (p)
Fe (d)
DOS
−10.0
−7.5
−5.0
−2.5
0.0
2.5
5.0
7.5
10.0
Energy (eV)
b. LiMn0.6Fe0.4PO4
Total DOS
Fe (d)
O (p)
Mn (d)
DOS
−10.0
−7.5
−5.0
−2.5
0.0
2.5
5.0
7.5
10.0
Energy (eV)

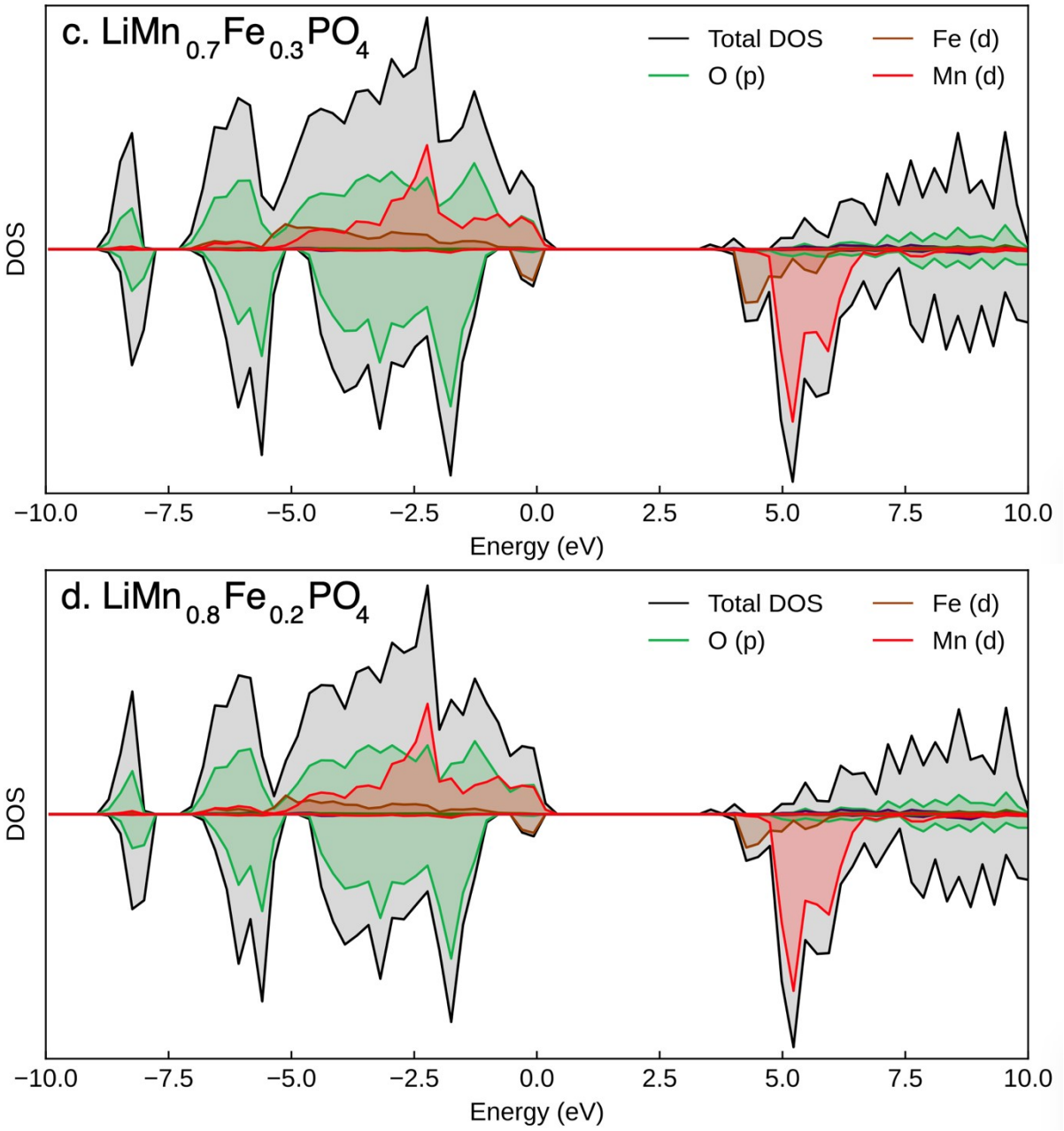

Figure S10: *Densities of states, as calculated in section 3.3, for a. $LiFePO_4$, b. $LiMn_{0.6}Fe_{0.4}PO_4$, c. $LiMn_{0.7}Fe_{0.3}PO_4$, d. $LiMn_{0.8}Fe_{0.2}PO_4$, and e. $LiMnPO_4$*

Electrode preparation and electrochemical measurements

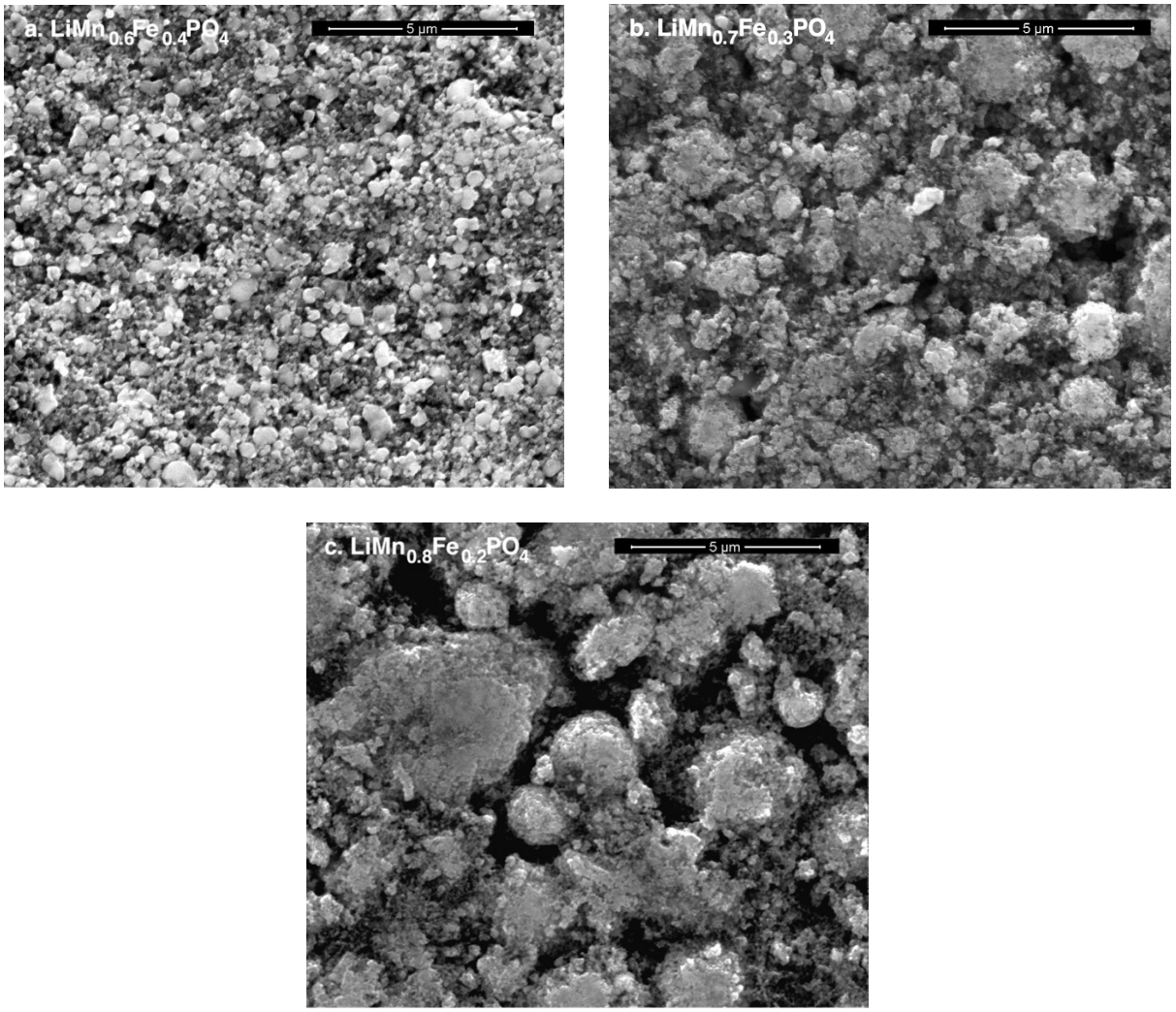

Figure S11: *SEM micrographs of a. $LiMn_{0.6}Fe_{0.4}PO_4$, b. $LiMn_{0.7}Fe_{0.3}PO_4$, c. $LiMn_{0.8}Fe_{0.2}PO$. Sub-micron particles seen for all three compositions; secondary agglomerates observed for the 70% and 80% Mn electrodes.*